Accepted Manuscript

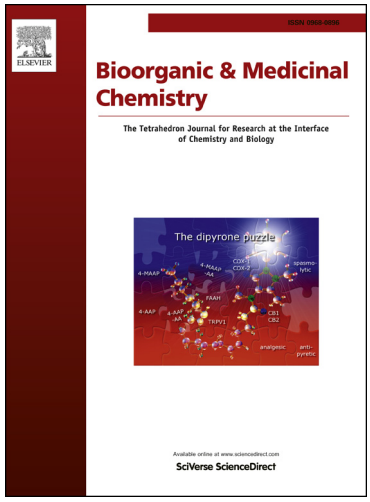

Synthesis and bio-evaluation of novel quinolino-stilbene derivatives as potential anticancer agents

Vandana Srivastava, Hoyun Lee

PII: S0968-0896(15)30132-2
DOI: http://dx.doi.org/10.1016/j.bmc.2015.11.007
Reference: BMC 12655

To appear in: *Bioorganic & Medicinal Chemistry*

Received Date: 31 August 2015
Revised Date: 29 October 2015
Accepted Date: 6 November 2015

Please cite this article as: Srivastava, V., Lee, H., Synthesis and bio-evaluation of novel quinolino-stilbene derivatives as potential anticancer agents, *Bioorganic & Medicinal Chemistry* (2015), doi: http://dx.doi.org/10.1016/j.bmc.2015.11.007

Synthesis and bio-evaluation of novel quinolino-stilbene derivatives as potential anticancer agents

Vandana Srivastava[1,2], Hoyun Lee[1,2,3*]

[1] Advanced Medical Research Institute of Canada, Health Sciences North, 41 Ramsey Lake Road, Sudbury, Ontario, Canada P3E 5J1
[2] Division of Medical Sciences, Northern Ontario School of Medicine, 935 Ramsey Lake Road, Sudbury, Ontario, Canada P3E 2C6
[3] Departments of Medicine, the University of Ottawa, Ottawa, Ontario K1H 5M8, Canada

***Corresponding author**
Hoyun Lee, Advanced Medical research Institute of Canada, 41 Ramsey Lake Road, Sudbury, Ontario, P3E 5J1, Canada. Phone: +1 705 522-6237, ext. 2703. E-mail: hlee@amric.ca

Running title: Anticancer activity of quinolino-stilbene derivatives

Abstract

A series of 25 novel quinolino-stilbene derivatives were designed, synthesized and evaluated for their potential as anticancer agents. Three of them not only displayed quite potent antiproliferative activity with IC_{50} values <4 μM but also showed approximately two-fold selectivity against cancer cells, compared to non-cancerous cells. Three other compounds exhibited comparatively good activity with IC_{50} values in the range of 4-10 μM, and the rest was moderately active or inactive. One of these viz. 3-[E-(4-fluorostyryl)]-2-chloroquinoline (compound **7B**) caused substantial DNA damage and arrested cell cycle in S phase. Interestingly, **7B** was very active against MDA-MB468 ($IC_{50=}$0.12 μM), but not against other cell lines examined. Compound 3-[Z-(3-(trifluoromethyl)styryl)]-2-chloroquinoline (**12A**), the most effective against all cancer cell lines examined, caused prolonged cell cycle arrest at mitosis and eventually apoptosis. Data from an *in vitro* study showed that compound **12A** inhibited microtubule polymerization in a similar fashion to nocodazole. Further study using *in silico* molecular modeling revealed that **12A** causes the impediment of microtubule polymerization by binding to tubulin at the same cavity where podophyllotoxin binds.

Key words:
Quinoline; stilbene; anticancer agent; tubulin; cell cycle; spindle checkpoint; apoptosis

1. Introduction

Cancer is the second most common cause of death in the United States, and the American Cancer Society estimates 1,658,370 new cases and 583,430 cancer-related deaths in 2015.[1] Although the development of early detection methods and timely intervention have resulted in the substantial improvement of survival and quality of life in certain cancer populations, effective cancer treatments are still difficult to achieve. One crucial limitation of current cancer therapies is that a curable dose often cannot be given due to severe side effects. Moreover, cancer curability is further hampered by the emergence of tumor cells that are resistant to therapeutic agents.[2] Therefore, there is a great need of developing new anticancer therapeutics with better pharmacological properties including increased selectivity for tumor cells. As a part of achieving this goal, we previously synthesized and characterized quinoline-based anticancer agents, some of which showed substantial promises.[3–6] Quinoline, a heterocyclic aromatic compound present in a wide range of natural and synthetic pharmaceuticals, is a privileged skeleton in drug discovery. Quinoline derivatives possess many different biological and pharmacological activities including antimicrobial, antimalarial, antifungal, anti-inflammatory, analgesic, antiviral, antiprotozoal, cardiovascular, CNS effective and antineoplastic.[7,8] Several well-known anticancer agents including camptothecin, topotecan and irinotecan contain a quinoline moiety.[9] It is also well-known that quinoline analogues often inhibit tubulin polymerization, DNA repair, tyrosine kinase activity, proteasome, histone acetyl-transferases (HATs) and histone deacetylase (HDACs), all of which are considered to be effective cancer therapeutic targets.[10]

Stilbenes (1,2 diarylethylene, Fig.1) attract considerable interest because of their wide range of biological activities and potential therapeutic values, especially against cancer.[11–15] E-Resveratrol (Fig. 1) is a phytoalexin stilbene found in berries, grapes, peanuts and red wine. Resveratrol and its analogues exhibit various biological and pharmacological activities including anticancer.[16–18] Combretastatin A4 (Fig. 1), isolated from *Combretum caffrum*, is another natural stilbene analogue possessing potent tubulin inhibition activity.[9,19] CA4P (combretastatin-4, 3-O phosphate), a prodrug of CA4, significantly reduces blood flow to the tumor cells, leading to extensive tumor necrosis. Several other stilbene derivatives have been synthesized previously in an attempt to develop effective anticancer drugs.[20–23] Tamoxifen (Fig. 1), one of the stilbene

derivatives, shows selective inhibition activity against estrogen receptor and is currently used as chemotherapeutic agent for breast cancer treatment.[24,25]

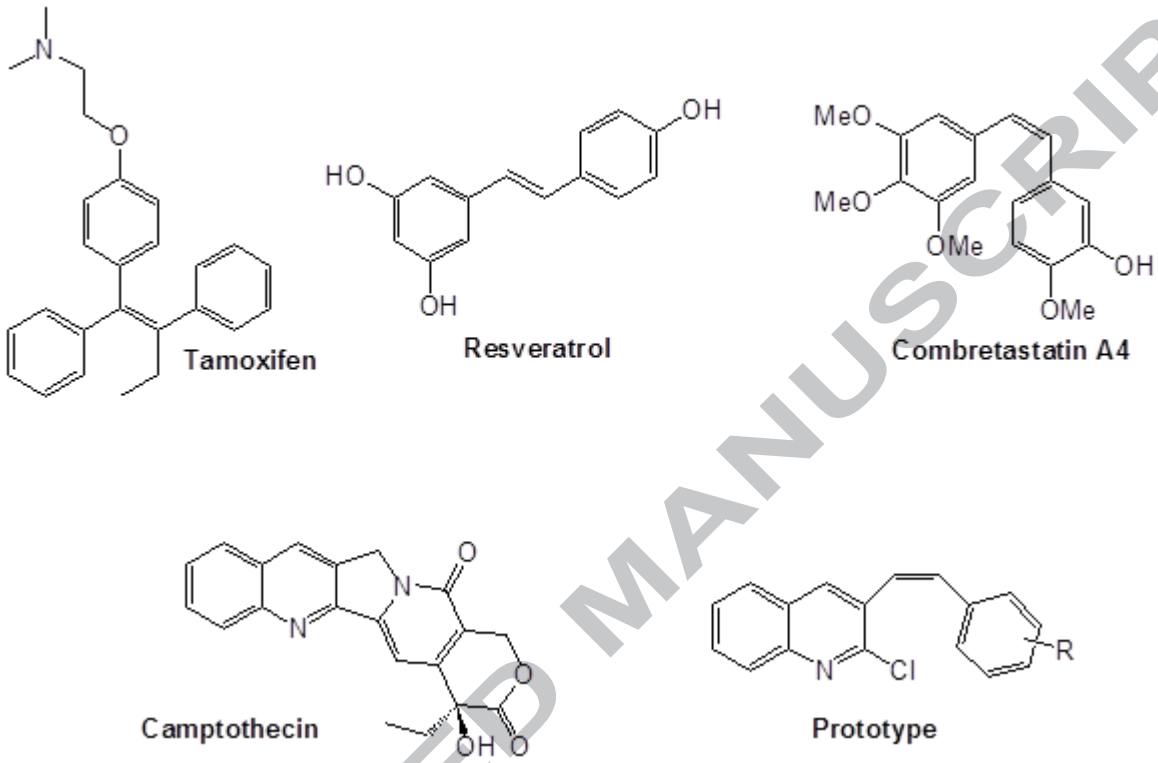

Figure 1. Prototype of quinoline-based stilbene derivatives. Shown are various stilbene derivatives being used as anticancer agents (tamoxifen, resveratrol and combretastatin A4) and the quinoline-based anticancer agent camptothesin.

The introduction of fluorine to bioactive molecules may alter their physiological properties and bioactivities. For instance, a fluorinated taxane is more active than the parental taxane against several cancer cell lines.[26] High electronegativity, chemical reactivity and the small size of fluorine all contribute to the enhancement of binding affinity, metabolic stability and selective target reactivity.[27] As the number of drug candidates with one or more fluorine atoms continues to increase in recent years, several groups have reviewed the role of fluorine in medicinal chemistry.[27–30]

To extend our ongoing efforts to develop effective and safe anticancer agents, we designed and synthesized a series of novel stilbene derivatives that are composed of a substituted quinoline moiety as ring A and a fluorine- or trifluoromethyl-substituted phenyl group as ring B. Subsequently, we examined their anticancer activities and cancer cell selectivity using four different cancer cell lines and a matching non-cancer cell line.

2. Result and discussion

2.1. Chemistry

All the quinolino-stilbene derivatives were synthesized by performing Wittig reactions on substituted quinoline-3-carbaldehyles (**5a-5d**), Wittig salts (**2**) using dimethyl sulfoxide as polar aprotic solvent, and sodium hydroxide as the base (Scheme1).[31] Quinoline-3-carbaldehydes (**5a-d**; Scheme 1) were either synthesized starting with substituted acetanilide (**4**) via Vilsmeier-Haack reaction using dimethylformamide (DMF) and phosphorus oxychloride ($POCl_3$) at 85^{o}C-90°C as described previously[32] or purchased from sigma. Benzyl triphenylphosphene bromide (Wittig salts, **2**) were synthesized by the reaction of corresponding benzyl bromides with triphenylphosphine and toluene under refluxing conditions. All of the final products were characterised by ^{1}H, ^{13}C NMR and mass spectroscopy, which were found to be consistent with the assigned structures (Table1).

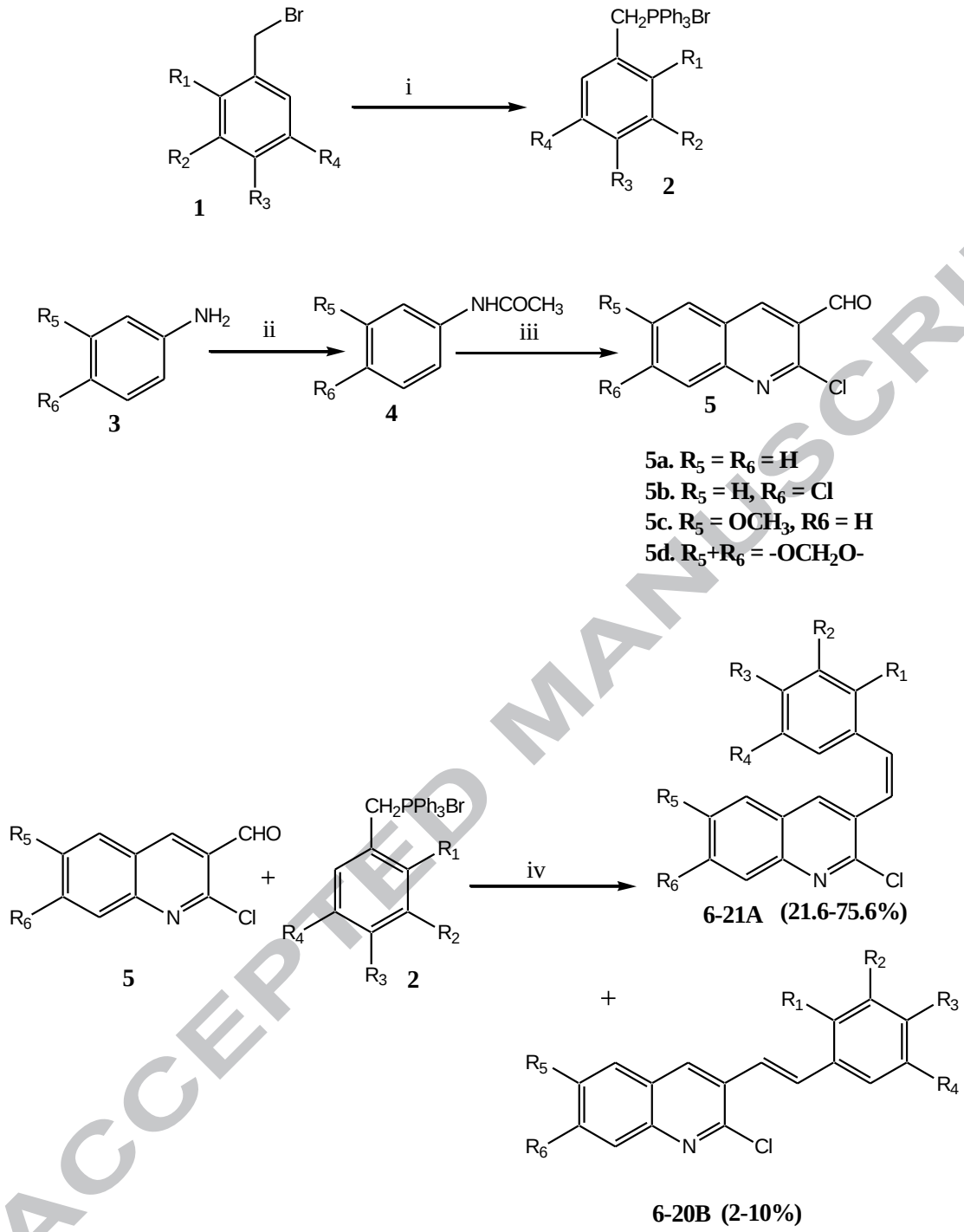

Scheme 1. Reagents and conditions: (i) PPh_3, toluene reflux; (ii) dil HCl, acetic anhydride, rt; (iii) $POCl_3$: DMF 3:1, ice, then 90°C, reflux; and (iv) NaOH, DMSO, rt.

Table 1: Chemical structures of novel stilbene derivatives

S. No	Compounds	$C_{17}H_6NClR_1R_2R_3R_4R_5R_6$					
		R_1	R_2	R_3	R_4	R_5	R_6
1	6A	H	H	CF_3	H	H	H
2	7A	H	H	F	H	H	H
3	7B	H	H	F	H	H	H
4	8A	H	H	CF_3	H	H	Cl
5	9A	H	H	F	H	H	Cl
6	10A	H	H	CF_3	H	OCH_3	H
7	10B	H	H	CF_3	H	OCH_3	H
8	11A	H	H	F	H	OCH_3	H
9	11B	H	H	F	H	OCH_3	H
10	12A	H	CF_3	H	H	H	H
11	12B	H	CF_3	H	H	H	H
12	13A	H	CF_3	H	H	OCH_3	H
13	14A	H	CF_3	H	CF3	OCH_3	H
14	14B	H	CF_3	H	CF3	OCH_3	H
15	15A	H	CF_3	H	CF3	H	H
16	16A	H	CF_3	H	CF3	H	Cl
17	17A	CF_3	H	CF_3	H	H	H
18	17B	CF_3	H	CF_3	H	H	H
19	18A	CF_3	H	CF_3	H	OCH_3	H
20	18B	CF_3	H	CF_3	H	OCH_3	H
21	19A	H	CF_3	H	CF3	$-OCH_2O-$	
22	19B	H	CF_3	H	CF3	$-OCH_2O-$	
23	20A	H	CF_3	H	H	$-OCH_2O-$	
24	20B	H	CF_3	H	H	$-OCH_2O-$	
25	21A	CF_3	H	H	H	OCH_3	H

Cis (**6A-21A**) and *trans* (**6B-20B**) isomers, the major and minor products of the Wittig reaction respectively, were purified by column chromatography. We sometimes encountered difficulties in separating these two stereoisomers due to their close retention factors (RFs), resulting in medium to low yield of pure isomers along with the mixture of isomers. In some cases only *cis* products were isolated in the pure chemical form. The geometry of stilbenes (*cis* and *trans*) was identify by ^{1}HNMR on the basis of H-H coupling constant (J). For some *cis* derivatives (for instance **12A**), we unexpectedly got only one signal for two ethylene protons when spectra were run in $CDCl_3$. On the other hand, two signals (one doublet, J = 15 Hz, & one merged doublet) for two ethylene protons were found for *trans* isomer (**12B**). The resultant mass spectra of both the isomers were in agreement with expected structures. To confirm geometry of

cis isomer, we ran the sample **12A** in acetone d6, by which we could clearly resolve doublets (J = 12.15 Hz) for two ethylene protons.

2.2. Biological activity

2.2.1. In vitro cytotoxicity and structural activity relationship (SAR)

We examined the novel compounds for their antiproliferative activities against four cancer cell lines: HeLa (cervical carcinoma), MDA-MB231 (ER-negative undifferentiated metastatic breast cancer), MCF7 (ER-positive well-differentiated breast cancer), and MDA-MB468 (PTEN mutated, intermediately differentiated breast cancer). To determine differential effects between cancer and non-cancer cells, we also examined the effect of these compounds on 184B5, a non-cancer breast epithelial cell line. Data from sulforhodamine B (SRB)-based assays[33] showed that the stilbene analogues displayed cell line-dependent IC_{50} values (Table 2). Three of the compounds examined (**12A**, **13A** and **21A**) showed IC_{50} values in the range of 2.6-4.0 μM against all four cancer cell lines. Furthermore, they were approximately two-fold more effective on cancer cells than non-cancerous cells (Table 2). Three of the derivatives (**6A**, **14A** and **15A**) were also relatively active with IC_{50} values in the range of 4-10 μM. The rest was generally not very active with IC_{50} of 10 μM or higher.

When considered in the context of SAR, the results suggest that stereochemistry and the positions of different functional groups are likely to play important roles in their activities. We found that the *cis* configuration of stilbene derivatives is generally more favorable for higher activity and better cancer selectivity than *trans*, except for **7B**. This data is in line with previous report indicating that s-*trans* conformation of chalcones possess better anti-invasive activities than s-*cis* counterpart. Indeed, the most anti-invasive compound shown in that study, which was geometrically similar to corresponding s-*trans* chalcone, was designed as *cis* (Z) stilbene mimic.[34] Compound **7B** (*trans*) was very active against MDA-MB468 (IC_{50}, 0.12 μM) and moderately active against MCF7 (IC_{50}, 15.13 μM) breast cancer cells. However, it was not active against HeLa, MDA-MB231 and 184B5 cells. This result suggests that SAR is substantially affected by the genetic background of the (tumor) cells. In this context, it may be worth to note that PTEN is mutated in the MDA-MB468 cell line.

Table 2: Antiproliferative activity of stilbene derivatives against cancer and non-cancer cells.

S. No	Compounds	IC_{50} Values in µM ±S.E.M. against different cell lines				
		HeLa	MCF7	MDA-MB231	MDA-MB468	184B5
1	6A	4.22±0.32	4.26±0.58	5.36±0.33	7.38±0.12	7.94±0.63
2	7A	24.91±1.89	20.29±2.30	23.98±0.14	5.29±0.83	35.73±1.00
3	7B	>50	15.13±5.79	>50	0.12±0.02	38.45±9.5
4	8A	12.64±0.22	6.45±1.24	13.55±4.12	16.13±0.46	26.40±0.61
5	9A	38.62±5.46	16.89±1.92	42.56±2.03	10.91±0.10	26.89±10.98
6	10A	16.21	12.41±1.99	22.83	22.65±1.94	40.04
7	10B	>50	46.97±2.93	48.83±1.56	>50	33.48±1.06
8	11A	9.67±0.84	8.97±3.03	11.40±0.02	15.17±1.06	19.18±1.4
9	11B	>50	14.05±3.61	11.03±1.28	14.84±3.66	9.74±1.8
10	**12A**	**2.85±0.02**	**3.53±0.74**	**3.75±0.29**	**3.70±0.37**	**6.15±0.40**
11	12B	20.27±0.27	24.43±3.64	45.01±2.08	23.99	24.73±3.8
12	13A	3.03±0.12	2.78±0.68	3.28±0.24	3.91±0.75	5.58±0.13
13	14A	4.14±0.30	4.70±1.21	4.47±0.11	5.79±0.63	7.97±1.95
14	15A	6.78±0.66	7.46±1.16	10.13±0.35	10.52±0.71	13.67±0.98
15	16A	41.35±6.50	41.71±4.41	>50	>50	42.95±11.43
16	17A	35.89±1.96	10.45	41.76±11.61		ND
17	18A	>50	>50	>50	>50	>50
18	19A	>50	>50	>50	>50	>50
19	20A	20.09±0.20	18.90±0.23	26.0±6.32	>50	16.97±0.13
20	21A	2.60± 0.08	4.47±0.08	2.77±0.08	4.98±0.80	5.31±0.71
21	Paclitaxel*	2.29±0.03	3.99±0.14	2.56±0.80	3.87±0.50	2.32±0.25
22	Camptothecin*	6.13±0.63	ND**	5.77	14.76±2.02	4.96±2.18
23	Chloroquine	29.96±3.39	ND	36.53±3.08	19.86±0.84	63.08

*IC_{50} in nM; ** Not determined

The presence of a CF_3 group on the phenyl ring generally renders good activity as shown by compounds **6A**, **12A**, **13A** and **21A**. The replacement of a CF_3 group with an F atom reduced the activity by 2-5 fold (**6A** *vs* **7A** and **8A** *vs* **9A**). An addition of a chlorine group at the position 7 (**8A**) or a methoxy group at the position 6 (**10A**) on the quinoline ring reduced the activity by 2-4 fold when combined with a 4 CF_3 substituted phenyl ring. The shift of the CF_3 group from

the position 4 (**6A**) on the benzene ring to the position 3 (**12A**) improved activity by ~2 fold. However, an addition of a methoxy group at the position 6 on the quinoline ring did not show any effect on the antiproliferative activity when combined with a CF_3 group on the phenyl ring (**12A** *vs* **13A**). The shift of a CF_3 group from the position 3 to the position 2 along with a methoxy group at the position 6 (**13A** *vs* **21A**) did not show any significant effect on the activity. The addition of one more CF_3 group on the phenyl ring affected the activity profile. The presence of CF_3 groups at the 3 and 5 positions rendered 5-10 fold better activity than presence at the 2 and 4 positions (**15A** *vs***17A** & **14A** *vs* **18A**). An addition of a chlorine group at the position 7 on the quinoline ring along with CF_3 groups at the 3 and 5 positions of the phenyl ring reduced the activity by ~5 fold (**15A** *vs* **16A**), whereas the addition of a methoxy group at the position 6 improved the activity by ~2 fold (**15A** *vs* **14A**). An addition of a methylenedioxy group on the quinoline ring reduced activity by ~10 fold (**19A** *vs* **20A**).

According to SAR studies, a CF_3 group at the position 2 or 3 of the phenyl ring is best suited for better antiproliferative activity. A methoxy group at the positon 6 of the quinoline ring is tolerable; however, it does not contribute to the enhancement of activity. Compound **12A**, the most active compound in this series was also examined for its activity against MCF10A, another non-cancer breast cell line. The IC_{50} value against MCF10A was 6.01±0.28 µM (Fig. 2), which is similar to that of 184B5 non-cancer cell line (Table 2). This result confirms that compound **12A** is selective for cancer cells in inhibiting cell proliferation. We carried out further biological studies with compound **12A**, the lead compound, and compound **7B** that showed high activity against MDA-MB468 cells.

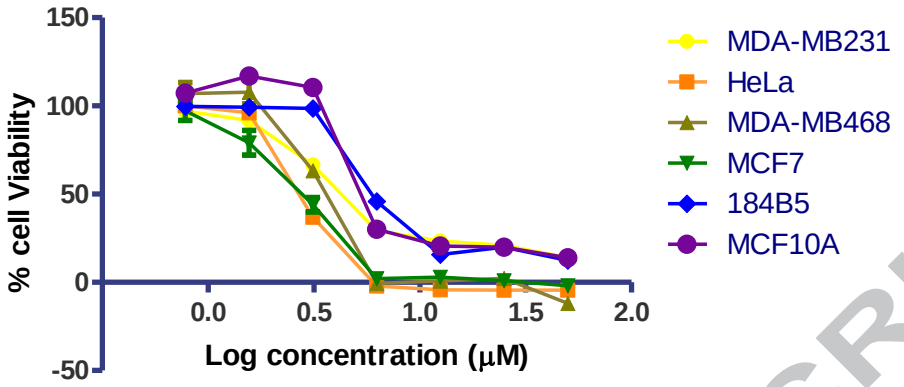

Figure 2. Antiproliferative effects of compound **12A** on cancer and matching non-cancer cell lines. An SRB assay was carried out with exponentially growing cells as described in Materials and methods.

2.2.2. Compounds 12A and 7B arrested cell cycle at mitosis and S-phase, respectively, eventually leading to cell death by apoptosis

When HeLa cells were treated with 6 μM of compound **12A**, the number of cells in G2-M was 78% by 12 h, a substantial increase from 19% shown in time 0 h (Fig. 3A, 12 h). By 24 h post-treatment, cells arrested at G2/M were substantially decreased, with a concomitant increase in cell population with sub-G1 DNA content (Fig. 3A, 24 h). Together, this data suggests that compound **12A** impedes normal G2-M progression, eventually leading to cell death as a cell tries to complete its cell division cycle without properly segregating its chromosomes. Compound **12A** also caused a similar pattern of G2/M arrest and DNA fragmentation in the MDA-MB231 metastatic breast cancer cells (Fig. 3B and Supplementary Fig. S1). In contrast, MCF10A, a non-cancer breast cell line, showed neither substantial G2/M arrest nor DNA fragmentation in the presence of compound **12A** (Fig. 3B and Supplementary Fig. S2).

The treatment of MDA-MB 468 cells with compound **7B** produced substantially increased S-phase population by 24 h (41.7%), compared to sham control (16.9%). The cell population in S phase was decreased by 48 h post-treatment with a concomitant increase in sub-G1 population, suggesting that a death pathway was activated in those cells arrested in S-phase without going through proper cell division process (Supplementary Fig. S3).

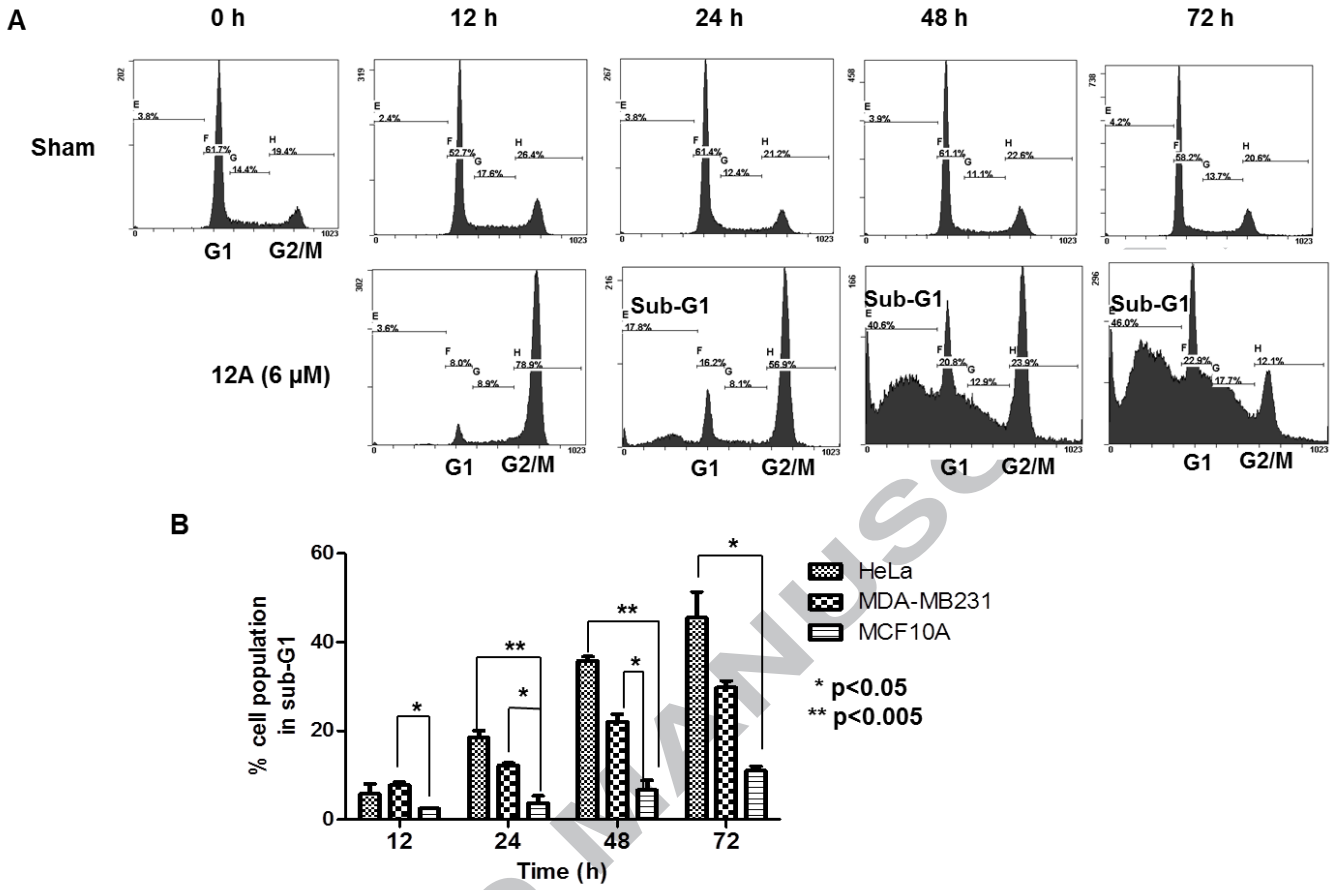

Figure 3. Compound **12A** caused cell cycle arrest at G2/M by 12 h and extensive cell death by 48 h post-treatment. (**A**) Flow cytometry profiles of asynchronous HeLa cells treated with **12A (**6 μM), which showed dramatic increases in sub-G1 population by 48 h post-treatment. Post-treatment time (h) shown is in hour(s). (**B**) % of sub-G1 population of cells at different time points. Data is from an average of two replicates of flow cytometry (as shown in panel A). Bars represent mean ±S.E.M. of two independent experiments.*p<0.05, **p<0.005.

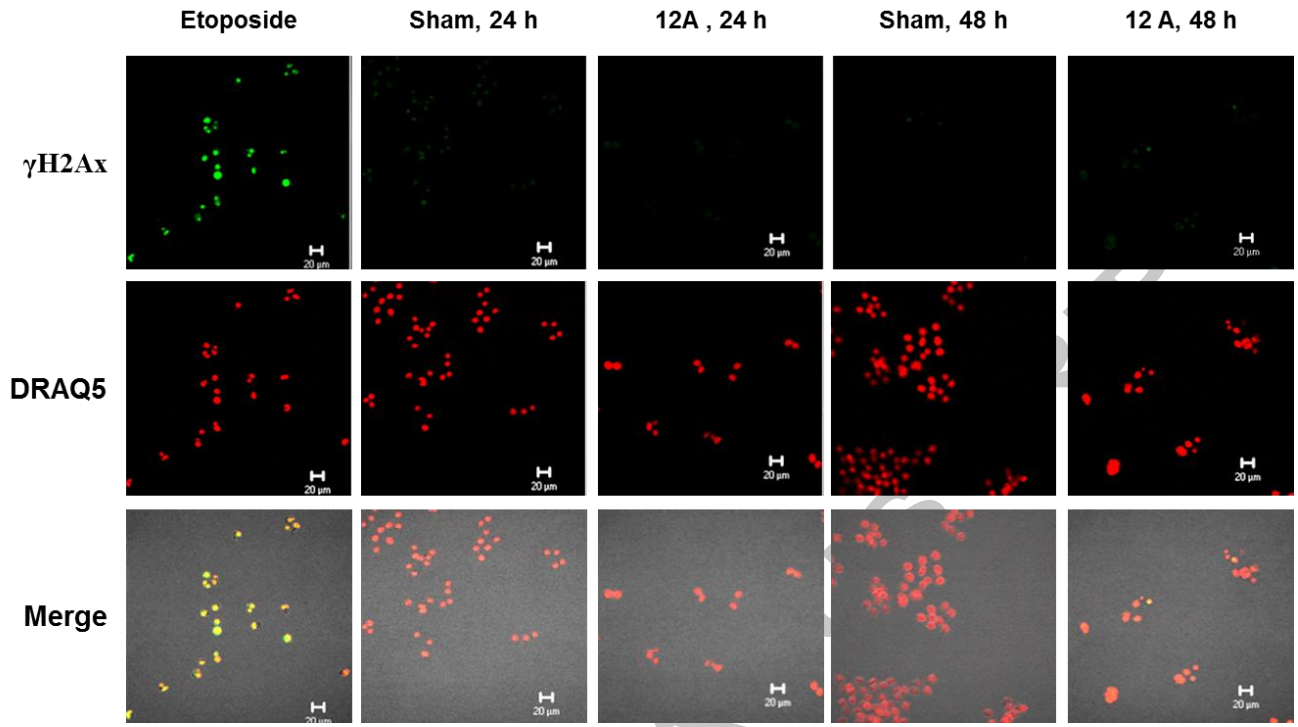

Figure 4. Compound **12A** did not cause DNA damage. HeLa cells were treated with 6 μM of **12A** or 50 μM etoposide for 24 or 48 h, followed by immunostaining with an anti-γH2A.X (phospho-Ser139) antibody. DNA was counterstained with DRAQ5. Scale bar is 20 μm

To determine if compounds **12A** and **7B** cause DNA damage, we carried out immunostaining of **12A**-treated HeLa cells and **7B**-treated MDA-MB468 cells with an anti-γH2A.X (phospho-Ser139) antibody. Data shown in Fig. 4 indicates that **12A** does not cause DNA damage at least up to 48 h post-treatment. Therefore, the arrest of cell cycle at G2/M observed by flow cytometry (Fig. 3A) is not caused by DNA damage. In contrast, MDA-MB468 cells treated with 1 μM **7B** showed substantial DNA damage as most of the treated cells showed γH2A.X positive by 24 h post-treatment (Supplementary Fig. S4). This data thus suggests that **7B** causes DNA damage which in turn causes S-phase arrest, eventually leading to cell death.

Cell cycle may be arrested at metaphase by the activation of spindle assembly checkpoint (SAC) for a variety of reasons.[35] To gain insight into whether **12A** caused cell-cycle arrest by SAC activation, we investigated the levels of (phosphorylated) proteins involved in the G2-M transition. We found that the protein level of Wee 1 kinase was barely detectable in the presence of **12A**, while the level of histone 3 phosphorylation on serine 10 was much higher than that of

control (Fig. 5A and B). This data is consistent with the notion that **12A**-treated cells have already passed G2 and chromosome condensation stage[36] by 12 h-post treatment. The level of cyclin B was very high in cells treated with **12A** at all of the time points examined (Fig. 5A and B). To our surprise, the level of cyclin B was still very high even at 48 h post-treatment when a large number of cells contained sub-G1 DNA content (Fig. 3A). These data indicate that cells were arrested prolonged duration at the spindle checkpoint step (Fig. 5A and B).

A large number of **12A**-treated cells contained sub-G1 DNA content by 48 h post-treatment, suggesting that they were dying by apoptosis (Fig. 5A). This conclusion was confirmed by the data that PARP1 protein was cleaved by 48 h post-**12A** treatment (Fig. 5A). We then documented **12A**-treated cells by a time-lapse camera. As expected, HeLa cells treated with **12A** showed severe membrane blebbing and popcorn-like morphology, a typical phenotype of cells undergoing apoptosis (Fig. 5C).[37]

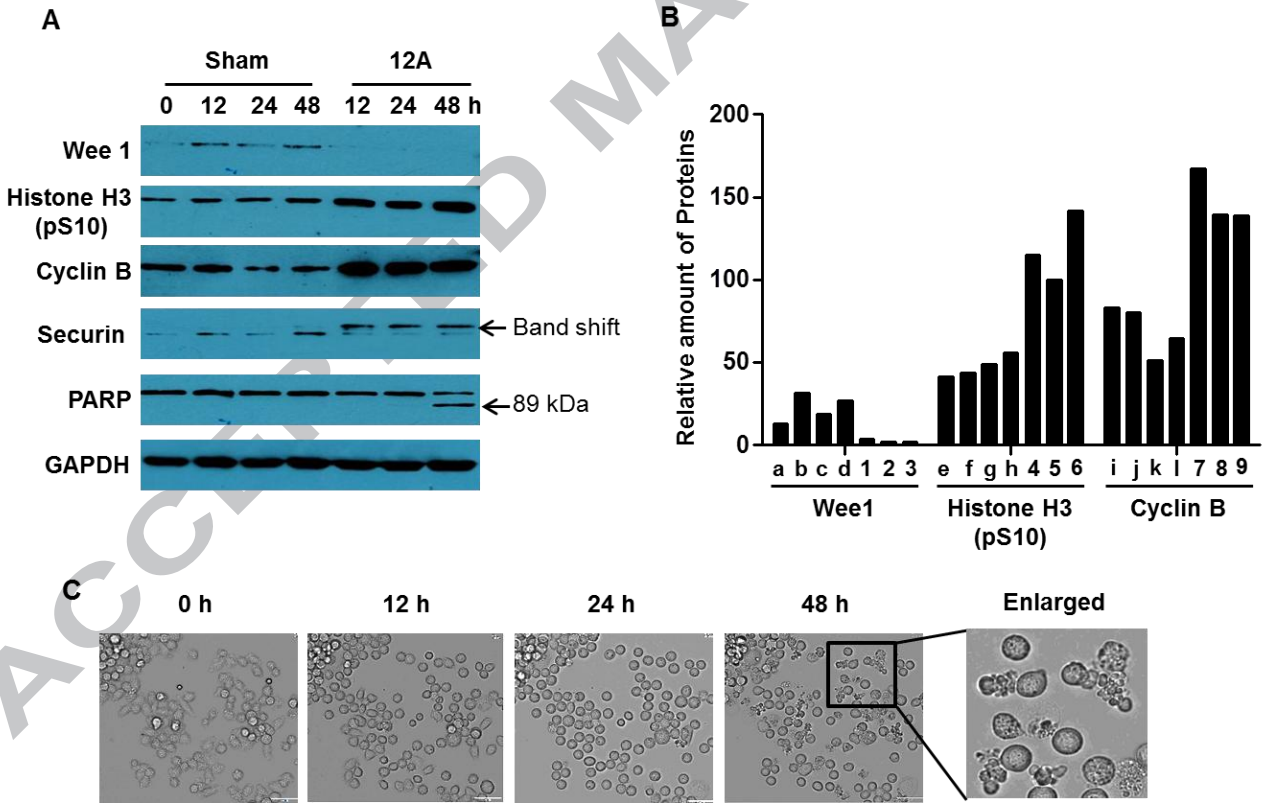

Figure 5. Cells arrested at mitosis by **12A** underwent massive apoptosis by 48 h post-treatment. (**A**) Western blot analysis indicates that cells are arrested at mitosis in the presence of **12A**. HeLa

cells were sham-treated or treated with 6 μM **12A**, and collected at indicated time points. Cell extracts were then subjected to polyacrylamide gel electrophoresis, followed by Western blotting with antibodies specific for proteins listed at the left of the panel. GAPDH is a loading control. (**B**) The relative abundance of proteins was normalized with that of GAPDH, and plotted in a graph form. (**C**) **12A** caused apoptosis. HeLa cells treated with **12A** were subjected to documentation by time-lapse microscopy. Slides shown are pictures taken at the indicated time points. Scale bar is 50 μm.

2.2.3. 12A-treated cells are defective in chromosome alignment and segregation

Interestingly, securin band was up-shifted in cells treated with **12A** (Fig. 5A), of which pattern is often observed in cells treated with microtubule-interacting drugs such as paclitaxel, colchicine and vinblastine.[38] Our data thus raised the possibility that **12A** might impede microtubule functions. To gain insights into this possibility, we examined cell morphology by immunofluorescence microscopy. By 12 h post-treatment, sham-treated cells were mostly in normal interphase morphology (Fig. 6A, Sham). In contrast, the majority of cell treated with **12A** were arrested at mitosis with disoriented tubulin structure (Fig. 6A, **12A**, α-tubulin stained cell). The chromosomes of cells exposed to **12A** were condensed, but not properly aligned at center plate (Fig. 6A, arrows). As their nuclear membrane was already broken (as evident by the lack of membrane staining by an anti-lamin A antibody), they have already entered mitosis. However, these mitotic cells were "permanently" arrested at mitosis as the entire chromosomes were not aligned at the centre plate (arrows in Fig. 6B and C).

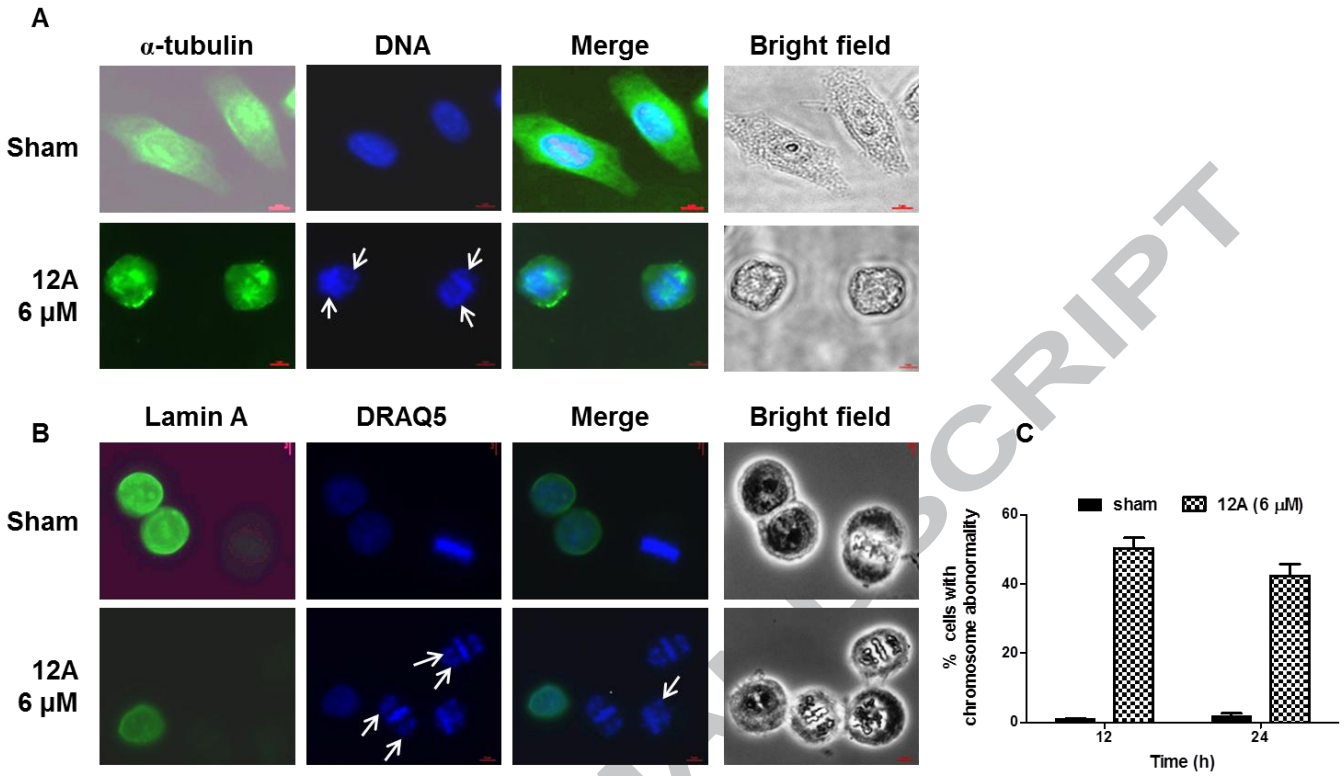

Figure 6. Compound **12A** caused defects in tubulin function and chromosome alignment at mitosis. (**A**) Cell morphology was abnormal in the presence of **12A**, likely due to defects in microtubule function. Pictures were taken 12 h post-treatment. DNA was stained with DAPI. Arrows show abnormal alignment of chromosomes. Scale bar is 5 μm. (**B**) Chromosome alignment at the center plate was not properly completed in the presence of **12A**. HeLa cells were analyzed 12 h post-treatment. DNA was counterstained with DRAQ5. Arrows show misaligned chromosomes. (**C**) Numbers of cells with defective chromosome alignment were quantified at 12 h and 24 h post-treatment. 100 cells were counted for each experiment, and the entire experiment was repeated once more.

2.2.4. 12A inhibits tubulin polymerization

Since securin band-shift (Fig. 5A) and data from immunofluorescence microscopy (Fig. 6) raised the possibility of **12A** being a microtubule interacting agent, we evaluated the effect of **12A** on tubulin polymerization with an *in vitro* tubulin assay kit. The kit was based on the

principle that light scatter by the microtubule is proportional to the concentration of polymerized microtubules, which can be detected at 340 nm wave-length. Therefore, tubulin stabilizing and destabilising agents would produce higher and lower absorbance, respectively, than the tubulin buffer control. As expected, paclitaxel and nocodazole (Noco) produced high and low absorbance at 340 nm, respectively, as the former stabilizes microtubules and the latter inhibits microtubule polymerization (Fig. 7). The absorbance pattern of **12A** at 6 and 12 µM was similar to that of nocodazole, indicating that it is an inhibitor of microtubule polymerization (Fig. 7). Taken together, our data indicated that the inhibition of microtubule polymerization by **12A** leads to prolonged cell cycle arrest at the mitotic spindle checkpoint stage, eventually resulting in apoptosis.

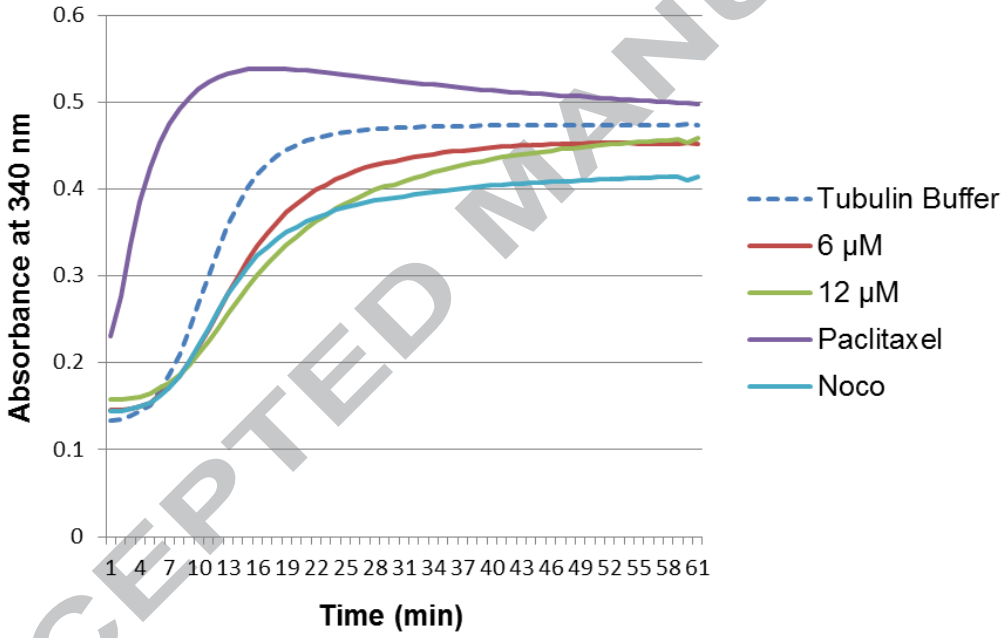

Figure 7. Compound **12A** inhibited tubulin polymerization. Microtubule polymerization kinetics are shown in the presence of different ligands: paclitaxel 10 µM, nocodazole (Noco) 5 µM, compound **12A** 6 µM or 12 µM. Tubulin buffer was used as a control.

2.2.5. The molecular target of 12A coincides with the podophyllotoxin (PDT)-binding site on the tubulin

Since our data is consistent with the notion that **12A** impedes tubulin polymerization, we searched for the potential binding site of **12A** on the tubulin using the MOE *Sitefinder* program (See Material and methods) and the co-crystalized structure of the tubulin α-β heterodimers (PDBID: 1SA1).[39] We found that the most likely **12A**-binding site determined by the lowest docking energy (S) and root mean square deviation (RMSD) coincides with the PDT binding pocket on the tubulin (Fig. 8): it shows the lowest S-score (-6.1615) and RMSD (0.0126). This modeling data predicts that compound **12A** forms a pi-bond interaction with amino acid asparagine B258 (Asn B258) with a bond length of 3.77Å and energy -0.6 kcal/mol (Fig. 8C). Potential Van der Waals interaction sites of amino acids lysine B352, asparagine B258, threonine A179, alanine B250, valine B315, alanine B316, leucines B255, B248 and B255, valine A181 and alanine B354 are common in **12A** and PDT binding interactions. PDT, a natural product belongs to lignan class of chemicals, exhibits strong anticancer activity against various cancer cell lines.[9] PDT, similarly to **12A**, interacts with tubulin, inhibits its assembly and arrests cell cycle in metaphase.

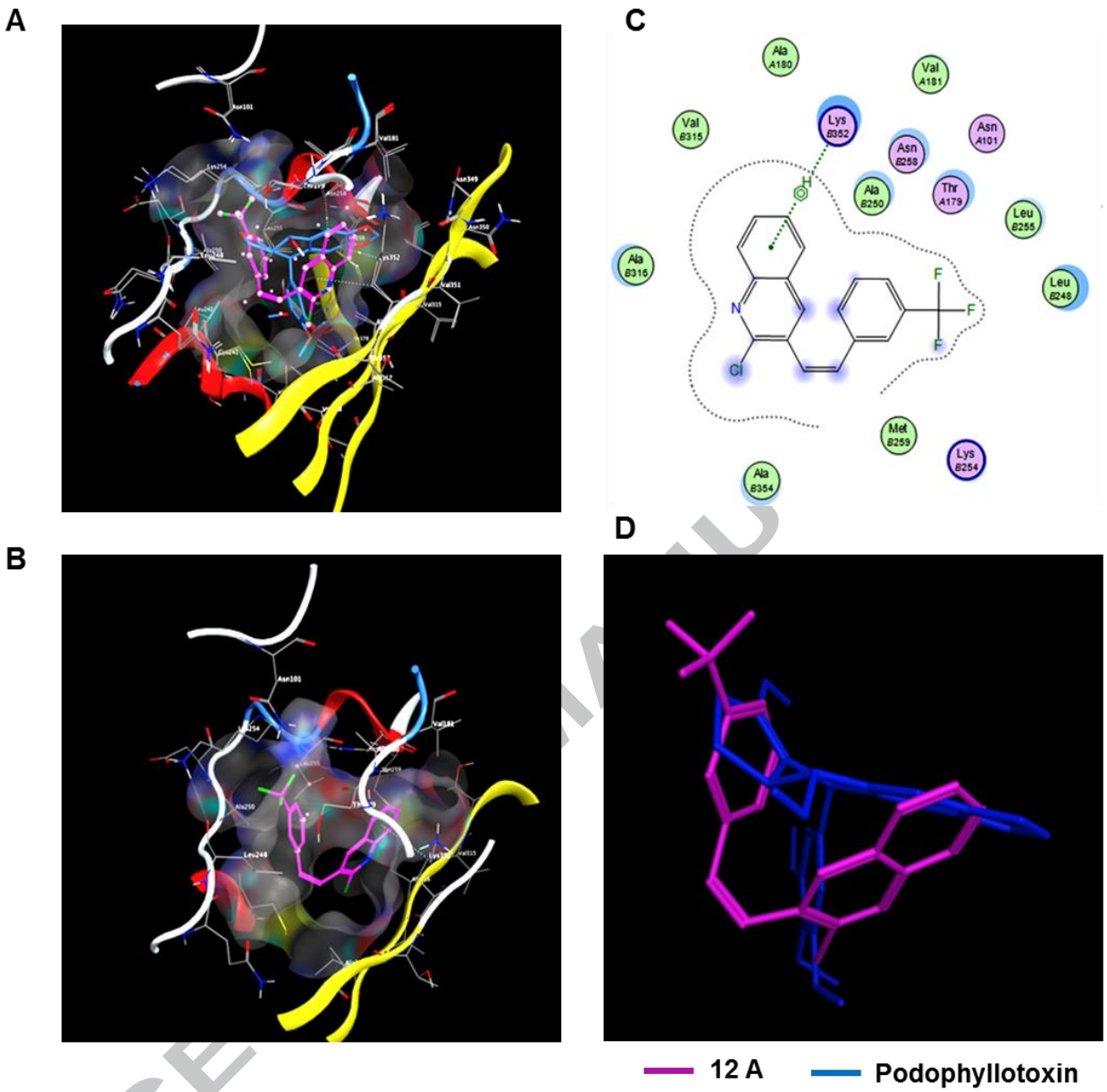

Figure 8. Data from *in silico* molecular modeling suggests that compound **12A** binds to tubulin at the same cavity bound by PDT. (**A**) An image of docking both **12A** (magenta) and PDT (blue) at the PDT-binding site on the tubulin. (**B**) An image of **12A** alone docking at the PDT-binding site on the tubulin. (**C**) Proximity contour of **12A** showing Van der Waals and pi-bond interactions with adjacent amino acid residues of tubulin in the PDT pocket. (**D**) The relative bindings of **12A** and podophyllotoxin at the PDT-binding cavity on the tubulin, which was derived from the figure in panel A.

3. Conclusion

A total of 25 novel quinolino-stilbene derivatives were designed and synthesized, among which 20 were studied for their antiproliferative activity. Although *trans* derivatives were generally less active, one of them, **7B**, showed surprisingly strong activity against MDA-MB468 breast cancer cells (IC_{50} = 0.12 μM). Data from flow cytometry and immunofluorescence microscopy suggested that **7B** causes considerable DNA damage, resulting cell cycle arrest in S-phase and eventually apoptosis. However, **7B** was not effective on other cell lines examined, indicating that genetic background is an important factor in its cell killing ability.

Some of the *cis* derivatives exhibited good anticancer activity against all four cancer cell lines examined. Three compounds in this series (**12A**, **13A**, **21A**) exhibited quite potent antiproliferative activities with IC_{50} less than 4 μM; three other compounds (**6A**, **14A** and **15A**) displayed relatively good antiproliferative activities with IC_{50} in the range of 4-10 μM. Compound **12A**, the most active one in this series, caused prolonged cell cycle arrest at the spindle checkpoint step, eventually leading to cell death by apoptosis. Data from Western blotting, an *in vitro* tubulin polymerization assay, and an immunofluorescence-based study strongly indicated that **12A** causes cell cycle arrest by impeding tubulin polymerization. The result of *in silico* molecular modeling is consistent with this conclusion, as the model predicts that **12A** binds to the pocket known to be bound by PDT. As **12A** preferentially kills cancer over non-cancer cells, it is a promising anticancer lead compound that can be further optimized to enhance anticancer activity and cancer selectivity.

4. Experimental

4.1. Chemistry

All the chemicals and dry organic solvents were purchased from Sigma-Aldrich or Fisher, and used without further purification. Thin layer chromatography (TLC, aluminum plate coated with silica gel 60 F254, 0.25 mm thickness, Sigma) was used to monitor the progress of reactions. Iodine vapour and/or UV light was used to detect products on TLC. Melting points were measured with Sturat SMP-20 instrument in open capillaries and were uncorrected. All the

1H and 13 Carbon NMR (Nuclear Magnetic Resonance) spectra were recorded either with a Bruker Avance 400 or 500 MHz spectrometer (Bruker Scientific Corporation Ltd., Switzerland). Tetramethylsilane or solvent signal was used as internal standard, and chemical shift is reported in part per million (ppm). Splitting patterns are defined as follows: s, for singlet; bs for broad singlet; d for doublet; t, for triplet, m for multiplet, and coupling constant (J) is reported in hertz (Hz). Mass spectra were carried out with a Kratos Concept 1-S high resolution magnetic sector mass spectrometer with electron impact to identify mass of synthesized compounds.

4.1.1. General procedure of Wittig salt (2) synthesis

1.0 mmol of corresponding benzyl bromide was dissolved in toluene with 1.2 mmole of triphenylphosphene. Reaction mixture was refluxed at 110ºC for 1-3 h; generated precipitate was filtered to get Wittig salt (**2**) in 60-80% yield.

4.1.2 .General synthetic procedure of compounds 6A and 6B

In a round-bottom flask, 1.56 mmol of Wittig salt **(2)** and 2.5 mmol sodium hydroxide were dissolved in 3 ml of dimethylsulfoxide (DMSO) and stirred for 30 min. To this reaction mixture, 1.3 mmol of 2-chloroquinoline-3-carbaldehyde was added, followed by stirring it for 5 h to overnight (~15 h) at room temperature. After completing the reaction, mixture was neutralized with diluted HCl and extracted with chloroform. Organic layer was washed with water and dried over anhydrous sodium sulfate; solvent was evaporated; and crude mixture was purified by silica gel column chromatography to purify *cis* and *trans* stilbene derivatives. 1H spectra of all the stilbenes are shown in supplementary information.

4.1.2.1. 3[Z-(4-(trifluoromethyl)styryl)]-2-chloroquinoline (6A). Solid; yield = 57.4%; mp. 89-91°C; ^{1}H NMR (400 MHz, $CDCl_3$): δ 6.86 (s, 2H), 7.26 (d, 2H, J = 8.0 Hz), 7.42 (d, 2H, J = 8Hz), 7.45 (t, 1H, J = 8Hz), 7.54 (d, 1H, J = 8Hz), 7.67 (1, 1H, J = 8Hz), 7.86, (s, 1H), 7.89 (d, 1H, J = 12 Hz); ^{13}C NMR (100 MHz, $CDCl_3$):δ 122.60, 125.42 (q, 2C, J = 4 Hz), 126.86, 127.27, 127.54, 127.59, 129.12, 129.12, 129.33, 129.41, 130.68, 131.89, 133.46, 138.40, 139.44, 147.03,

150.28; MS (EI) 333.1 (M^+); HRMS calculated for $C_{18}H_{11}ClF_3N$ $[M]^+$ 333.05321, found $[M]^+$ 333.05436.

4.1.2.2. 3[Z-(4-fluorostyryl)]-2-chloroquinoline (7A). Solid; yield = 21.6%; mp. 86-88°C; ^{1}H NMR (400 MHz, $CDCl_3$): δ 6.69 (d, 1H, J=12Hz), 6.78 (d, 1H, J=12Hz), 6.86 (m, 2H), 7.13 (m, 2H), 7.44 (t, 1H, J=8.1Hz), 7.54 (d, 1H, J=8.1Hz), 7.65 (t, 1H, J=8.5Hz), 7.90 (s, 1H), 7.98 (d, 1H, J=8.36Hz); ^{13}C NMR (100 MHz, $CDCl_3$):δ 115.43, 115.65, 125.37, 126.95, 127.13, 127.58, 128.27, 129.79, 130.45, 130.56, 130.64, 131.82 (d, J =3.75 Hz), 132.22, 138.37, 146.89, 150.54, 160.85 (d, J=246Hz); MS (EI) 283.1 (M^+); HRMS Calculated for $C_{17}H_{11}ClFNO$ $[M]^+$ 283.05641, found $[M]^+$ 283.06003.

4.1.2.3. 3-[E-(4-fluorostyryl)]-2-chloroquinoline (7B). Solid; yield = 5.4%; mp. 144-146°C; ^{1}H NMR (400 MHz, $CDCl_3$): δ 7.05 (t, 2H, J=8.0Hz), 7.13 (d, 1H, J=16.0Hz), 7.41 (d, 1H, J=16.0Hz), 7.55 (m, 3H), 7.67 (t, 1H, J=8.0Hz), 7.82 (d, 1H, J=8.0Hz), 7.98 (d, 1H, J=8.0Hz), 8.65 (s,1H); ^{13}C NMR (100 MHz, $CDCl_3$):δ 115.79, 116.00, 123.32, 123.34, 127.24, 127.53, 128.36, 128.58, 128.66, 130.20, 130.29, 132.03, 132.79, 133.69, 146.87, 150.17, 161.66 (d, J=248Hz);); MS (EI) 283.1 (M^+); HRMS calculated for $C_{17}H_{11}ClFNO$ $[M]^+$ 283.05641, found $[M]^+$ 283.05303.

4.1.2.4. 3-[Z-(4-(trifluoromethyl)styryl)]-2,7-dichloroquinoline (8A). Solid; yield = 26.9%; mp. 121-124°C; ^{1}H NMR (500 MHz, $CDCl_3$): δ 6.85 (d, 1H, J = 12.1Hz), 6.91 (d, 1H, J = 12.1Hz), 7.29 (d, 2H, J = 8.5Hz), 7.46 (m, 4H), 7.86 (s, 1H), 8.02 (d, 1H, J = 1.7Hz); ^{13}C NMR (125 MHz, $CDCl_3$): δ 122.82, 125.19, 125.51 (q, 2C, J = 3.75 Hz), 127.25, 127.38, 128.39, 128.66, 128.97, 129.11, 129.11, 129.60, 132.24, 136.71, 138.08, 139.30, 147.23, 151.50; MS (EI) 367.0 (M^+); HRMS calculated for $C_{18}H_{10}Cl_2F_3N$ $[M]^+$ 367.01424, found $[M]^+$ 367.02624.

4.1.2.5. 3-[Z-(4-fluorostyryl)]-2,7-dichloroquinoline (9A). Solid; yield = 22.6%; mp. 103-105°C; ^{1}H NMR (500 MHz, $CDCl_3$): δ 6.71 (d, 1H, J = 12.1 Hz), 6.84 (d, 1H, J = 12.1 Hz), 6.89 (t, 2H, J = 8.7Hz), 7.15 (m, 2H), 7.45 (d, 1H, J = 8.7 Hz), 7.51 (d, 1H, J = 8.7Hz), 7.91 (s, 1H), 8.01 (s, 1H); ^{13}C NMR (125 MHz, $CDCl_3$): δ 99.99, 115.52, 115.69, 125.05, 125.28, 127.35, 128.24, 128.61, 130.07, 130.54, 130.61, 132.58, 136.45, 138.05, 147.09, 151.75, 161.15 (d, J =

246.84 Hz); MS (EI) 317.0 (M^+); HRMS calculated for $C_{17}H_{10}ClFN$ $[M]^+$ 317.01743, found $[M]^+$ 317.0174.

4.1.2.6. 3-[Z-(4-(trifluoromethyl)styryl)]-2-chloro-6-methoxyquinoline (10A). Solid; yield = 75.6%; mp. 127-129°C; ^{1}H NMR (400 MHz, $CDCl_3$): δ 3.87 (s, 3H), 6.82 (d, 1H, J=2.5Hz), 6.85 (s, 2H), 7.31 (d, 2H, J=8.0Hz), 7.36 (dd, 1H, J=9 &2.5Hz), 7.46 (d, 2H, J=8.0Hz), 7.79 (s, 1H), 7.91 (d, 1H, J = 9.0Hz); ^{13}C NMR (125 MHz, $CDCl_3$):δ 55.58, 104.92, 122.88, 123.39, 125.43 (q, 2C J=3.75Hz), 127.83, 127.99, 129.16, 129.16, 129.48, 129.48, 129.66, 136.67, 137.11, 139.52, 143.09, 147.55, 153.29;); MS (EI) 363.1 (M^+); HRMS calculated for $C_{19}H_{13}ClF_3NO$ $[M]^+$ 363.06378, found $[M]^+$ 363.06483.

4.1.2.7. 3-[E-(4-(trifluoromethyl)styryl)]-2-chloro-6-methoxyquinoline(10B). Solid; yield = 8.6%; mp. 129-131°C; ^{1}H NMR (500 MHz, $CDCl_3$): δ 3.96 (s, 3H), 7.11 (d, 1H, J=2.5Hz), 7.18 (d, 1H, J=16.0Hz), 7.36 (dd, 1H, J= 9.0 &2.5Hz), 7.58(d, 1H, J=16.0Hz), 7.68 (s, 4H), 7.89 (d, 1H, 9.0Hz), 8.29 (s, 1H); ^{13}C NMR (125 MHz, $CDCl_3$):δ 55.61, 105.05, 123.00, 123.31, 125.79(q, 2C, J=3.75Hz), 126.22, 127.07, 127.07, 128.50, 129.66, 129.71, 130.01, 131.37, 132.95, 139.99, 143.17, 147.46, 158.42;MS (EI) 363.1 (M^+); HRMS calculated for $C_{19}H_{13}ClF_3NO$ $[M]^+$ 363.06378, found $[M]^+$ 363.06473.

4.1.2.8. 3-[Z-(4-fluorostyryl)]-2-chloro-6-methoxyquinoline (11A). Solid; yield = 33.9%; mp. 134-136°C; ^{1}H NMR (500 MHz, $CDCl_3$): δ 3.86 (s, 3H), 6.71 (d, 1H, J=10Hz), 6.80 (d, 2H, J=10Hz), 6.89 (t, 1H, J=8.7Hz)7.16 (m, 2H), 7.34 (dd, 1H, J=10Hz), 7.84 (s, 1H), 7.90 (d, 1H, J=10Hz); ^{13}C NMR (125 MHz, $CDCl_3$):δ55.57, 104.88, 115.41, 115.58, 123.15, 125.55, 128.04, 129.63, 129.94, 130.58, 130.65, 131.90, 131.98, 137.08, 142.95, 147.82, 158.91, 161.07 (d, J=246.25 Hz); MS (EI) 313.1 (M^+); HRMS calculated for $C_{18}H_{13}ClFNO$ $[M]^+$ 313.06697, found $[M]^+$ 313.06504.

4.1.2.9. 3-[E-(4-fluorostyryl)]-2-chloro-6-methoxyquinoline (11B). Solid; yield = 6.5%; mp. 185-189°C; ^{1}H NMR (500 MHz, CD_3OD): δ 3.84 (s, 3H), 6.71 (d, 1H, J=15Hz), 6.90 (d, 1H, J=10Hz), 7.06 (t, 2H, J=10Hz), 7.18 (t, 2H, J = 10Hz), 7.30 (d, 1H, J = 5Hz), 7.42 (dd, 1H,J = 10Hz), 7.86 (d, 1H, J = 10Hz), 8.09 (s, 1H); ^{13}C NMR (125 MHz, CD_3OD):δ 56.11, 106.26,

115.89, 116.06, 123.63, 125.79, 128.58, 129.51, 130.36, 131.13, 131.19, 132.40, 132.44, 137.73, 142.68, 147.13, 158.33, 160.89 (d, J=243.75); MS (EI) 313.1 (M^+); HRMS calculated for $C_{18}H_{13}ClFNO$ $[M]^+$ 313.06697, found $[M]^+$ 313.06575.

4.1.2.10. 3-[Z-(3-(trifluoromethyl)styryl)]-2-chloroquinoline (12A). Solid; yield = 57.5%; mp. 86-89°C; ^{1}H NMR (500 MHz, Acetone D_6): δ 6.94 (d, 1H J = 12.15 Hz), 7.05 (d, 1H, J = 12.15 Hz), 7.43 (t, 1H, J = 7.6 Hz), 7.49 (d, 1H, J = 7.7 Hz), 7.54 (m, 3H), 7.78 (m, 2H), 7.96 (d, 1H, J = 8.45), 816 (s, 1H); ^{13}C NMR (125 MHz, $CDCl_3$):δ 122.75, 124.34 (q, J = 3.75 Hz), 125.82 (q, J = 3.75 Hz), 126.82, 127.19, 127.23, 127.44, 128.28, 128.92, 129.19, 130.63, 130.95, 131.77, 131.83, 136.61, 138.30, 147.01, 150.30;MS (EI) 333.1 (M^+); HRMS calculated for $C_{18}H_{11}ClF_3N$ $[M]^+$ 333.05321, found $[M]^+$ 333.05651.

4.1.2.11. 3-[E-(3-(trifluoromethyl)styryl)]-2-chloroquinoline (12B). Solid; yield = 6.9%; mp. 108-111°C; ^{1}H NMR (500 MHz, $CDCl_3$): δ 7.20 (d, 1H, J = 15.0Hz), 7.53 (m, 4H), 7.21 (t, 1H, J = 10Hz), 7.78 (d, 1H, J = 10Hz), 7.82, (s, 1H), 7.86 (d, 1H, J = 10Hz), 8.02 (d, 1H, J = 10Hz), 8.40 (s, 1H); ^{13}C NMR (125 MHz, $CDCl_3$):δ 122.91, 123.77 (q, J = 3.75), 124.99 (q, J = 3.75Hz), 125.41, 127.43, 127.43, 127.62, 128.37, 129.35, 129.71, 129.82, 130.55, 131.23 131.65, 134.12, 137.33, 147.05, 150.07;MS (EI) 333.1 (M^+); HRMS calculated for $C_{18}H_{11}ClF_3N$ $[M]^+$ 333.05321, found $[M]^+$ 333.05670.

4.1.2.12. 3-[Z-(3-(trifluoromethyl)styryl)]-2-chloro-6-methoxyquinoline (13A). Solid yield = 73.1%; mp. 130-135°C: ^{1}H NMR (500 MHz, $CDCl_3$): δ3.86 (s, 3H), 6.81 (d, 1H,J = 2.5Hz), 6.86 (s, 2H), 7.28 (d, 1H, J = 7.5Hz), 7.32 (m, 2H), 7.46 (d, 1H, J = 7.5Hz 7.53 (s, 1H), 7.82 (s, 1H), 7.90 (d, 1H, J = 10Hz);^{13}C NMR (125 MHz, $CDCl_3$): δ 55.57, 104.86, 122.78, 123.35, 124.29 (q, J=3.75 Hz), 125.85 (q, J=3.75 Hz), 127.40, 127.95, 128.89, 129.34, 129.65, 130.90 (q, J = 31.25Hz), 131.55, 131.88, 136.66, 137.00, 143.09, 147.59, 158.28;MS (EI) 363.1 (M^+); HRMS calculated for $C_{19}H_{13}ClF_3NO$ $[M]^+$ 363.06378, found $[M]^+$ 363.06246.

4.1.2.13. 3-[Z-(3,5-bis(trifluoromethyl)styryl)]-2-chloro-6-methoxyquinoline (14A). Solid; yield = 73.9%; mp. 139-141°C; ^{1}H NMR (500 MHz, $CDCl_3$): δ 3.86 (s, 3H), 6.81 (d, 1H, J=2.6Hz), 6.86 (d, 1H, J=12.2 Hz), 6.98 (d, 1H, J=12.2Hz), 7.37 (dd, 1H, J=9.2 &2.1Hz), 7.66 (s,

2H), 7.71 (s, 1H), 7.81 (s, 1H), 7.91 (d, 1H, J=9.2Hz);^{13}C NMR (125 MHz, $CDCl_3$):δ 55.58, 104.69, 121.19 (m), 121.89,121.89, 123.74, 127.77, 128.35, 128.86 (2C, bS), 129.26, 129.70, 129.84, 131.47, 136.71, 137.95, 143.27, 147.18, 158.45; MS (EI) 431.1 (M^+); HRMS calculated for $C_{20}H_{12}ClF_6NO$ $[M]^+$ 431.05116, found $[M]^+$ 431.05265.

4.1.2.14. 3-[E-(3,5-bis(trifluoromethyl)styryl)]-2-chloro-6-methoxyquinoline (14B). Solid yield = 2.1%; mp. 170-172°C; ^{1}H NMR (500 MHz, $CDCl_3$): δ 3.93 (s, 3H, $-OCH_3$), 7.14 (d, 1H, J = 2.5Hz), 7.24 (d, 1H, J = 15 Hz), 7.41 (dd, 1H, J = 2.5 & 9.2Hz) 7.67 (d, 1H, J = 15Hz), 7.85 (s, 1H), 9.95 (d, 1H, J = 9.0Hz), 8.01 (s, 2H), 8.34 (s, 1H); MS (EI) 431.1 (M^+); HRMS calculated for $C_{20}H_{12}ClF_6NO$ $[M]^+$ 431.05116, found $[M]^+$ 431.05083.

4.1.2.15. 3-[Z-(3,5-bis(trifluoromethyl)styryl)]-2-chloroquinoline (15A). Solid; yield = 33.5%; mp. 103-105°C; ^{1}H NMR (500 MHz, $CDCl_3$): δ6.89 (d, 1H, J=12.2 Hz), 7.00 (d, 1H, J=12.2 Hz), 7.50 (t, 1H, J=7.5Hz), 7.57 (d, 1H, J=7.5Hz), 7.65 (s, 2H), 7.71 (s, 1H), 7.73 (t, 1H, J=8.25Hz), 7.90 (s, 1H), 8.03 (d, 1H J=8.45Hz) ^{13}C NMR (125 MHz, $CDCl_3$): δ 121.23 (m), 121.86, 121.86, 126.60, 127.29, 127.48, 128.23, 128.81(bs, 2C), 129.06, 130.07, 131.80 (2C), 137.90, 138.08, 147.17, 149.90; MS (EI) 401.0 (M^+); HRMS Calculated for $C_{19}H_{10}ClF_6N$ $[M]^+$ 401.04060, found $[M]^+$ 401.04327.

4.1.2.16. 3-[Z-(3,5-bis(trifluoromethyl)styryl)]-2,7-dichloroquinoline (16A). Solid, yield =24.7%; mp. 138-139°C: ^{1}H NMR (500 MHz, $CDCl_3$): δ 6.91 (d, 1H, J = 12Hz), 6.97 (d, 1H, J = 12Hz), 7.46 (d, 1H, J = 10Hz), 7.50 (d, 1H, J = 12 Hz), 7.63 (s, 2H), 7.72 (s, 1H), 7.87 (s, 1H), 8.02 (s, 1H); MS (EI) 435.0 (M^+); HRMS calculated for $C_{19}H_9Cl_2F_6N$ $[M]^+$ 435.00162, found $[M]^+$ 435.00456.

4.1.2.17. 3-[Z-(2,4-bis(trifluoromethyl)styryl)]-2-chloroquinoline (17A). Solid; yield = 26.7%; mp. 147-150°C; ^{1}H NMR (500 MHz, $CDCl_3$): δ 7.07 (d, 1H, J=12.0Hz), 7.15 (d, 1H, J = 12.0 Hz), 7.23 (d, 1H, J=10Hz), 7.47 (m, 3H), 7.60 (s, 1H), 7.70 (t, 1H, J = 10Hz), 9.99 (d, 2H, J = 12Hz); ^{13}C NMR (125 MHz, $CDCl_3$): δ 122.36, 123.44 (m), 124.54, 126.71, 127.34, 127.56, 128.26, 128.56 (bs), 128.93, 129.64, 129.82, 129.88, 130.15, 130.84, 131.86, 133.72, 133.98,

147.00, 150.12; MS (EI) 401.0 (M^+); HRMS calculated for $C_{19}H_{10}ClF_6N$ $[M]^+$ 401.0406, found $[M]^+$ 401.03806.

4.1.2.18. 3-[E-(2,4-bis(trifluoromethyl)styryl)]-2-chloroquinoline (17B). Solid; yield = 5.7%; mp. 165-167°C; ^{1}H NMR (500 MHz, $CDCl_3$): δ 7.54 (d, 1H, J=15Hz), 7.61 (m, 2H), 7.76 (t, 1H J=5Hz), 7.88 (d, 1H, J = 5Hz), 7.91 (d, 1H, J = 10Hz), 7.99 (m, 3H), 8.41 (s, 1H); ^{13}C NMR (125 MHz, $CDCl_3$): δ 122.27 , 123.41 (m), 124.44 , 127.19, 127.30, 127.58, 127.87, 128.21, 128.39, 128.51, 128.96 (bs), 129.10, 130.03, 130.35, 130.99, 134.90, 139.14, 147.37, 149.89;MS (EI) 401.0 (M^+); HRMS calculated for $C_{19}H_{10}ClF_6N$ $[M]^+$ 401.0406, found $[M]^+$ 401.04026.

4.1.2.19. 3-[Z-(2,4-bis(trifluoromethyl)styryl)]-2-chloro-6-methoxyquinoline (18A). Solid; yield = 57.4%; mp. 140-143°C; ^{1}H NMR (500 MHz, $CDCl_3$): δ 3.84 (s, 3H), 6.74 (d, 1H, J=2.5Hz), 7.04 (d, 1H, J=12Hz), 7.12 (d, 1H, J=12Hz), 7.23 (d, 1H, 8.1Hz), 7.33 (dd, 1H, J = 9.2&2.6Hz), 7.48 (md, 2H, J=7Hz), 7.87 (d, 1H, J=9.2Hz), 7.98 (s, 1H); ^{13}C NMR (125 MHz, $CDCl_3$):δ 55.58, 104.92, 122.39, 123.39 (m), 124.57, 127.86, 128.51(bs), 128.70, 129.60, 129.60, 129.77, 129.84, 130.07, 131.94, 131.94, 137.45, 139.04, 143.04, 147.39, 158.35; MS (EI) 431.1 (M^+); HRMS Calculated for $C_{20}H_{12}ClF_6NO$ $[M]^+$ 431.05116, found $[M]^+$ 431.05484.

4.1.2.20. 3-[E-(2,4-bis(trifluoromethyl)styryl)]-2-chloro-6-methoxyquinoline (18B). Solid; yield = 4.5%; mp. 175-177°C; ^{1}H NMR (500 MHz, $CDCl_3$): δ 3.98 (s, 3H), 7.16 (d, 1H, J=2.5Hz), 7.39 (dd, 1H, J=9.1 & 2.6Hz), 7.52 (d, 1H, J = 16Hz), 7.59 (d, 1H, J = 16Hz), 7.87 (d, 1H, J = 8.3Hz), 7.91 (d, 1H, J = 9.1Hz), 7.98 (s, 1H), 8.01 (d, 1H, J = 8.1Hz), 8.30 (s, IH); ^{13}C NMR (125 MHz, $CDCl_3$):δ55.67, 105.13, 122.27, 123.41 (m), 123.86, 124.57, 126.95, 128.19, 128.44, 128.98 (bs), 129.12, 129.70, 130.03, 130.17, 130.30, 133.62, 139.18, 143.54, 147.27, 158.54; MS (EI) 431.1 (M^+); HRMS calculated for $C_{20}H_{12}ClF_6NO$ $[M]^+$ 431.05116, found $[M]^+$ 431.05378.

4.1.2.21. 3-[Z-(3,5-bis(trifluoromethyl)styryl)]-2-chloro-6,7-methelenedioxyquinoline (19A). Solid; yield = 64%; mp. 164-165°C; ^{1}H NMR (500 MHz, $CDCl_3$): δ 6.21 (s, 2H), 6.77 (s, 1H), 6.83 (d, 1H, J = 12.1 Hz), 6.95 (d, 1H, J = 12.1Hz), 7.30 (s, 1H), 7.65 (s, 2H), 7.69 (d, 2H, J = 12.8 Hz); ^{13}C NMR (125 MHz, $CDCl_3$): δ 102.16. 102.19, 105.06, 121.08 (m), 121.91, 121.91,

123.72, 126.05, 128.82, 128.82 (bs), 129.19, 129.41, 131.71 (2C), 136.64, 138.08, 145.73, 147.67, 148.59, 152.00; MS (EI) 445.0 (M^+); HRMS calculated for $C_{20}H_{10}ClF_6NO_2$ $[M]^+$ 445.03043, found $[M]^+$ 445.02965.

4.1.2.22. 3-[E-(3,5-bis(trifluoromethyl)styryl)]-2-chloro-6,7-methelenedioxyquinoline (19B). Solid; yield = 5.2%; mp. 201-204°C; ^{1}H NMR (500 MHz, $CDCl_3$): δ 6.17 (s, 2H), 7.11 (s, 1H), 7.19 (d, 1H, J = 16.2 Hz), 7.33 (s, 1H), 7.63 (d, 1H, J = 16.2 Hz), 7.83 (s, 1H), 7.99 (s, 2H), 8.23 (s, 1H); MS (EI) 445.0 (M^+); HRMS calculated for $C_{20}H_{10}ClF_6NO_2$ $[M]^+$ 445.03043, found $[M]^+$ 445.03337.

4.1.2.23. 3-[Z-(3-(trifluoromethyl)styryl)]-2-chloro-6,7-methelenedioxyquinoline (20A). Solid; yield = 64%; mp. 123-125°C; ^{1}H NMR (500 MHz, $CDCl_3$): δ 6.10 (s, 2H), 6.77 (s, 1H), 6.83 (s, 2H), 7.26 (d, 1H, J=10Hz), 7.29 (s, 1H), 7.32 (d, 1H, J = 7.85 Hz), 7.45 (d, 1H, J=10Hz), 7.50 (s, 1H), 7.69 (s, 1H); ^{13}C NMR (125 MHz, CD_3OD):δ 102.06, 102.30, 105.00, 122.77, 123.88, 124.22 (q, J=3.75), 125.76 (q, J=3.75), 127.01, 127.30, 128.85, 130.86, 131.13, 131.89, 136.76, 137.00, 145.45, 148.00, 148.37, 151.71;MS (EI) 377.0 (M^+).

4.1.2.24. 3-[E-(3-(trifluoromethyl)styryl)]-2-chloro-6,7-methelenedioxyquinoline (20B). Solid; yield = 10%; mp. 162-164°C; ^{1}H NMR (500 MHz, $CDCl_3$): δ 6.12 (s, 2H), 7.05 (s, 1H), 7.10 (d, 1H, J=15Hz), 7.26 (s, 1H), 7.49 (m, 2H), 7.56 (d, 1H, J = 10 Hz), 7.74 (d, 1H, J=5Hz), 7.78 (s, 1H), 8.15 (s, 1H); ^{13}C NMR (125 MHz, CD_3OD):δ 102.11, 102.49, 105.03, 122.96, 123.61 (q, J=5Hz), 124.47, 124.76 (q, J=3.75), 125.37, 127.42, 129.29, 129.69, 130.53, 131.15, 132.82, 137.46, 145.42, 147.80, 148.53, 151.67; MS (EI) 377.0 (M^+); HRMS calculated for $C_{19}H_{11}ClF_3NO_2$ $[M]^+$ 377.04304, found $[M]^+$ 377.04464.

4.1.2.25. 3-[Z-(2-(trifluoromethyl)styryl)]-2-chloro-6-methoxyquinoline (21A). Solid; yield = 46.3%; mp. 143-145°C; ^{1}H NMR (500 MHz, $CDCl_3$): δ 3.83 (s, 3H), 6.70 (d, 1H, J = 2.5Hz), 6.95 (d, 1H, J = 11.95), 7.10 (d, 1H, J = 7.70 Hz), 7.15 (d, 1H, J = 11.95 Hz), 7.22 (t, 1H, J = 7.5 Hz), 7.28 (m, 2H), 7.52 (s, 1H), 7.24 (d, 1H, J = 7.85), 7.86 (d, 1H, J = 9.25); ^{13}C NMR (125 MHz, $CDCl_3$):δ 55.52, 105.07, 123.07, 123.17, 125.99 (q, J = 5.3Hz), 127.53, 127.92, 128.19,

128.74, 129.35, 129.54, 130.29, 131.13, 131.73, 135.19, 137.51, 142.86, 147.80, 158.18; MS (EI) 377.0 (M^+); HRMS calculated for $C_{19}H_{13}ClF_3NO$ $[M]^+$ 363.06378, found $[M]^+$ 363.06815.

4.2. Biological experiments

All of the cell lines used were purchased from ATCC and authenticated using a short tandem repeat (STR) profiling method by Genetica DNA Laboratories (Burlington, NC) (March 2015; July 2015). HeLa, MDA-MB231 and MDA-MB468 were grown in RPMI 1640 and MCF7 in DMEM. The culture media were supplemented with 10% fetal bovine serum (FBS) and a combination of penicillin (100 units/ml) and streptomycin (100 µg/ml). Non-cancer cells (MCF10A and 184B5) were grown in DMEM/F12 supplemented with 10% FBS, 20 ng/ml epidermal growth factor, 10 µg/ml insulin, 0.5 g/ml hydrocortisone and a combination of penicillin (100 units/ml) and streptomycin (100 µg/ml). Cells were grown under humidified condition at 37ºC with 5% CO_2 and 95% air.

4.2.1. Sulforhodamine B (SRB) cell proliferation assay

Antiproliferative activities of compounds were examined by an SRB assay as described previously.[33] Briefly, 4,000-5,000 cells/well were incubated for 16 h in a 96-well clustered plate. After 16 h of incubation, culture medium was replaced with fresh medium containing different dilutions of test compounds dissolved in DMSO. Some wells were treated with 100 µl of 10% trichloroacetic acid (TCA) as a negative control, and a sham (medium with DMSO) treated sample was used as a positive control. Culture medium was removed after 72 h of incubation, and cells were fixed with 10% TCA at 4ºC for 1 h. TCA was removed and cells were washed with cold tap water, and plate was air-dried, followed by addition of 50 µl of 0.4% SRB staining solution to each well. After 30 min incubation, SRB staining solution was removed. Cells were washed with 1% acetic acid solution, and then washed with tap water to remove unbound SRB, followed by air-drying. 200 µl of 10 mmol (pH 10.5) trizma base buffer was added to each well to solubilise cells, and plate was then read at 540 nm wave-length using an automated plate reader (Synergy H4 Hybrid Multi-Mode Microplate Reader, BioTek). Cell growth was calculated by the following formula: % cells proliferation = [(AT−CT)/ (ST−CT)] x100

Where AT is absorbance of treated cells; CT is absorbance of negative control cells; and ST is absorbance of sham treated cells. IC_{50} values were calculated from sigmoidal dose-response curves generated by two independent biological replicates, with four technical replicates in each set by using Graph Pad Prism v.5.04 software.

4.2.2. Cell cycle analysis

Approximately1×10^6 cells per plate were seeded overnight. Cells were then treated the next morning with test compounds, and harvested at scheduled time points post-treatment. Cell pellet was collected by centrifugation at 1,100 rpm (Allegra^{TM} X-12 centrifuge, Beckman Coulter) for 5min followed by washing twice with PBS, and fixing cells with 75% ethanol for 12-24 h at -20ºC. Ethanol was removed by centrifugation at 1,100 rpm (Allegra^{TM} X-12 centrifuge) for 5 min, and cells were suspended in PBS and centrifuged again 1,100 rpm (Allegra^{TM} X-12 centrifuge) for 5 min. PBS was removed and cell pellet was resuspended in propidium iodide (PI) staining solution containing 0.3% nonidet P-40,100 µg/ml RNase A and 100 µg/ml PI in PBS for 1 h. DNA content in the different phase of the cell cycle was analysed by flow cytometry using a Beckmann Coulter Cytomics FC500.

4.2.3. Western blot analysis

Samples treated with compound **12A** and sham control were collected at scheduled time points post-treatment and centrifuged for 5 min. at 1,100 rpm (Allegra^{TM} X-12 centrifuge, Backman Coulter). Cell pellets were washed with PBS by centrifugation for 5 min. at 1,100 rpm (Allegra^{TM} X-12 centrifuge), and were then lysed with 100 µl Lysis buffer (150 mmol NaCl, 5 mmol EDTA, 1% triton X-100, 10 mmol tris pH 7.4, 1 mmol PMSF, 5 mmol EDTA and 5 mmol protease inhibitors cocktail) by maintaining on ice for 10-15 min, followed by centrifugation at 1,100 rpm (Allegra^{TM} X-12 centrifuge) for 10 min at 4 ºC. Supernatant was collected and protein concentration was determined using a BCA protein assay kit (Thermo Scientific, USA). Cell lysates were diluted with 2× Laemmli sample buffer, and then boiled at 95-100ºC for 5 min. 30-40 µg protein was resolved by polyacrylamide gel (8 or 10%) electrophoresis. The resolved proteins were transferred to a PVDF membrane using a semi-dry gel transfer apparatus (75 min

at 24 volts), followed by "blocking" with 5% skim milk for 1 h. Proteins on the membrane were then incubated with primary antibody in 0.1% TBST buffer containing 5% skim milk for overnight at 4ºC. Membrane was washed three times with 0.1% TBST buffer and incubated with secondary antibody in TBST buffer containing 5% skim milk for 1 h. Finally, the membrane was washed with TBST buffer thrice, and signals were visualised on X-ray film using an ECL chemiluminescence kit (Super Signal West pico, Thermo Scientific, USA). Antibodies used were purchased from Abcam (Canada) or Santa Cruz biotechnology (Canada).

4.2.4. Immunofluorescence

Cells grown on sterile glass coverslips for 12-16 h were treated with test compounds for 12 and 24 h. At scheduled time points post-treatment, cells were permeabilized and fixed with 100% ice-cold methanol for 10-15 min at -20 ºC. Cells were then washed twice with 0.1% PBST buffer (0.1% Triton X 100 in PBS), and blocked with 1% FBS in TBST for 1 h, followed by incubation with a primary antibody (1:200 dilution in TBST) overnight at 4ºC. After washing with PBST three times for 5 min each, cells were incubated with a secondary antibody conjugated with fluorophore for 1 h. DNA was counterstained with DAPI or DRAQ5. After washing with PBST three times, coverslips were mounted onto glass-microscope slides with 9:1 glycerol: PBS solution. Images were captured using a Carl Zeiss Axioscope and analysed with ZEN pro 2012 software (Carl Zeiss International).

4.2.4. Tubulin polymerization assay

The effect of **12A** on tubulin polymerization was examined with a HTS-tubulin polymerization assay kit (Cytoskeleton USA), as per the supplier's protocol. In brief, 6 and 12 µM of **12A**, 10 µM paclitaxel (stabilizing agent), 5 µM nocodazole (polymerization inhibitor) and tubulin buffer alone (80 mmol PIPES, 2.0 mmol $MgCl_2$, 0.5 mmol EGTA, pH 6.9) were placed in 96-well microtiter plate, and incubated at 37ºC for 2-3 min. To this, 4 mg/ml tubulin dissolved in tubulin buffer (80 mmol PIPES, 2.0 mmol $MgCl_2$, 0.5 mmol EGTA, 1 mmol GTP, 10% glycerol, pH 6.9) was added and mixed for 5 s. Finally, polymerization kinetic was measured every min for 1 h at 340 nm wave-length using an automated plate reader (Synergy H4 Hybrid Multi-Mode

Microplate Reader, BioTek). Absorbance at 340 nm has been plotted against time to produce a time-dependent curve.

4.3 Molecular Modeling

Molecular modeling was performed with the Molecular Operating Environment system (MOE, Chemical Computing Group, Montreal, Canada). The structure of α/β tubulin heterodimer co-crystalized with PDT (podophyllotoxin) and other ligand was retrieved from protein data base (PDB ID: 1SA1). Ligands were removed and protein was protonated, side chain was fixed and energy minimization was done during structure preparation. All the other parameters were used default values. Protocol for docking was adopted from MOE website, and an induced-fit protocol was used (http://www.chemcomp.com/MOE-Structure_Based_Design.htm). Molecular modeling was validated by docking PDT to its known binding pocket. Twenty four different possible configurations of **12A** ligand were generated, and the best one was chosen on the basis of the lowest RMSD value and S-score.

Acknowledgement

Authors are grateful to Gerardo Ulibarri (Laurentian University) for allowing us to use their NMR facility, and John T. Arnason (University of Ottawa) for providing mass spectrometry data. The authors also gratefully acknowledge the generous financial supports from Northern Cancer Foundation, Northern Ontario Heritage Funds Corporation and the City of Greater Sudbury Development Corporation through the Northeastern Ontario Cancer Therapeutics Research Initiative (CTRI) project to HL.

References

1. American Cancer Society **2015**.

2. Holohan, C.; Van Schaeybroeck, S.; Longley, D. B.; Johnston, P. G. *Nat. Rev. Cancer* **2013**, *13*, 714–726.

3. Hu, C.; Raja Solomon, V.; Cano, P.; Lee, H. *Eur. J. Med. Chem.* **2010**, *45*, 705–709.

4. Zhang, H.; Solomon, V. R.; Hu, C.; Ulibarri, G.; Lee, H. *Biomed. Pharmacother.* **2008**, *62*, 65–69.

5. Solomon, V. R.; Hu, C.; Lee, H. *Eur. J. Med. Chem.* **2010**, *45*, 3916–3923.

6. Solomon, V. R.; Hu, C.; Lee, H. *Bioorg. Med. Chem.* **2010**, *18*, 1563–72.

7. Marella, A.; Tanwar, O. P.; Saha, R.; Ali, M. R.; Srivastava, S.; Akhter, M.; Shaquiquzzaman, M.; Alam, M. M. *Saudi Pharm. J.* **2013**, *21*, 1–12.

8. Kumar, S.; Bawa, S.; Gupta, H. *Mini-Reviews Med. Chem.* **2009**, *9*, 1648–1654.

9. Srivastava, V.; Negi, A. S.; Kumar, J. K.; Gupta, M. M.; Khanuja, S. P. S. *Bioorg. Med. Chem.* **2005**, *13*, 5892–908.

10. Solomon, V. R.; Lee, H. *Curr. Med. Chem.* **2011**, *18*, 1488–1508.

11. Inayat-Hussain, S. H.; Thomas, N. F. *Expert Opin. Ther. Pat.* **2004**, *14*, 819–835.

12. Hart, J. H. *Annu. Rev. Phytopathol.* **1981**, *19*, 437–458.

13. Roman, B. I.; De Coen, L. M.; Thérèse F C Mortier, S.; De Ryck, T.; Vanhoecke, B. W. A.; Katritzky, A. R.; Bracke, M. E.; Stevens, C. V *Bioorg. Med. Chem.* **2013**, *21*, 5054–63.

14. Gosslau, A.; Pabbaraja, S.; Knapp, S.; Chen, K. Y. *Eur. J. Pharmacol.* **2008**, *587*, 25–34.

15. Kumar, A. S.; Reddy, M. A.; Jain, N.; Kishor, C.; Murthy, T. R.; Ramesh, D.; Supriya, B.;

Addlagatta, A.; Kalivendi, S. V; Sreedhar, B. *Eur. J. Med. Chem.* **2013**, *60*, 305–24.

16. Kasiotis, K. M.; Pratsinis, H.; Kletsas, D.; Haroutounian, S. A. *Food Chem. Toxicol.* **2013**, *61*, 112–20.

17. Aggarwal, B. B.; Bhardwaj, A.; Agarwal, R. S.; Seeram, N. P.; Shishodia, S.; Takada, Y. *Anticancer Res.* **2004**, *24*, 2783–2840.

18. Saiko, P.; Szakmary, A.; Jaeger, W.; Szekeres, T. *Mutat. Res.* **2008**, *658*, 68–94.

19. Tron, G. C.; Pirali, T.; Sorba, G.; Pagliai, F.; Busacca, S.; Genazzani, A. A. *J. Med. Chem.* **2006**, *49*, 3034–3044.

20. Barrett, I.; Carr, M.; Boyle, N. O.; Greene, L. M.; Knox, A. J. S.; Lloyd, D. G.; Zisterer, D. M.; Meegan, M. J. *J. Enzym. Inhib. Med. Chem.* **2010**, *25*, 180–194.

21. Rajak, H.; Dewangan, P. K.; Patel, V.; Jain, D. K.; Singh, A.; Veerasamy, R.; Sharma, P. C.; Dixit, A. *Curr. Pharm. Des.* **2013**, *19*, 1923–55.

22. Wen, Z.; Xu, J.; Wang, Z.; Qi, H.; Xu, Q.; Bai, Z.; Zhang, Q.; Bao, K.; Wu, Y.; Zhang, W. *Eur. J. Med. Chem.* **2015**, *90C*, 184–194.

23. Pérez-Melero, C.; Maya, a. B. S.; Del Rey, B.; Peláez, R.; Caballero, E.; Medarde, M. *Bioorganic Med. Chem. Lett.* **2004**, *14*, 3771–3774.

24. Dhingra, K. *Invest. New Drugs* **1999**, *17*, 285–311.

25. Jordan, V. C. *Nat. Rev. Drug Discov.* **2003**, *2*, 205–213.

26. Ojima, I. *Chembiochem* **2004**, *5*, 628–35.

27. Hagmann, W. K. *J. Med. Chem.* **2008**, *51*, 4359–4369.

28. Isanbor, C.; O'Hagan, D. *J. Fluor. Chem.* **2006**, *127*, 303–319.

29. Böhm, H.-J.; Banner, D.; Bendels, S.; Kansy, M.; Kuhn, B.; Müller, K.; Obst-Sander, U.; Stahl, M. *Chembiochem* **2004**, *5*, 637–43.

30. Filler, R.; Saha, R. *Future Med. Chem.* **2009**, *1*, 777–791.

31. Srivastava, V.; Darokar, M. P.; Fatima, A.; Kumar, J. K.; Chowdhury, C.; Saxena, H. O.; Dwivedi, G. R.; Shrivastava, K.; Gupta, V.; Chattopadhyay, S. K.; Luqman, S.; Gupta, M. M.; Negi, A. S.; Khanuja, S. P. S. *Bioorg. Med. Chem.* **2007**, *15*, 518–25.

32. Srivastava, A.; Singh, R. *Indian J. Chem.* **2005**, *44 B*, 1868–1875.

33. Vichai, V.; Kirtikara, K. *Nat. Protoc.* **2006**, *1*, 1112–6.

34. Roman, B. I.; Ryck, T. De; Dierickx, L.; Vanhoecke, B. W. a.; Katritzky, A. R.; Bracke, M.; Stevens, C. V. *Bioorg. Med. Chem.* **2012**, *20*, 4812–4819.

35. Musacchio, A.; Salmon, E. D. *Nat. Rev. Mol. Cell Biol.* **2007**, *8*, 379–393.

36. Hans, F.; Dimitrov, S. *Oncogene* **2001**, *20*, 3021–3027.

37. Elmore, S. *Toxicol. Pathol.* **2007**, *35*, 495–516.

38. Tseng, H.-H.; Chuah, Q.-Y.; Yang, P.-M.; Chen, C.-T.; Chao, J.-C.; Lin, M.-D.; Chiu, S.-J. *PLoS One* **2012**, *7*, e36006.

39. Ravelli, R. B. G.; Gigant, B.; Curmi, P. A.; Jourdain, I.; Lachkar, S.; Sobel, A.; Knossow, M. *Nature* **2004**, *428*, 198–202.

Graphical Abstract